Ocean-Land-Atmosphere Research
A SCIENCE PARTNER JOURNAL

RESEARCH ARTICLE

Contrasting Anthropogenic Drivers Behind Asymmetric Warming in the Arctic and Antarctica

Basudev Swain[1*], Marco Vountas[2], Aishwarya Singh[3], Upasana Panda[4], Rui Song[5], Nidhi L. Anchan[6], Chakradhar Reddy Malasani[7], Dukhishyam Mallick[8], Richard Alawode[2], Adrien Deroubaix[9], Luca Lelli[10], Julia Schmale[11], Ankit Tandon[12], Sachin S. Gunthe[7], Manfred Wendisch[13], Vittal Hari[14], and Hartmut Bösch[2]

[1]Atmospheric, Oceanic and Planetary Physics, University of Oxford, Oxford, UK. [2]Institute of Environmental Physics, University of Bremen, Bremen, Germany. [3]Max Planck Institute for Chemistry, Biogeochemistry Department, Mainz, Germany. [4]Kalinga Institute of Industrial Technology (KIIT) Deemed to be University, Bhubaneswar, India. [5]National Centre for Earth Observation, Atmospheric, Oceanic and Planetary Physics, University of Oxford, Oxford, UK. [6]Department of Energy, Environmental, and Chemical Engineering, Washington University in Saint Louis, St. Louis, MO, USA. [7]Department of Civil Engineering, Indian Institute of Technology Madras, Chennai, India. [8]IJCLab Orsay, CNRS/IN2P3, Université Paris-Saclay, Paris, France. [9]Max-Planck-Institut für Meteorologie, Hamburg, Germany. [10]Remote Sensing Technology Institute, German Aerospace Centre (DLR), Wessling, Germany. [11]Extreme Environments Research Laboratory, École Polytechnique Fédérale de Lausanne, Lausanne, Switzerland. [12]Department of Environmental Sciences, Central University of Jammu, Samba, Jammu& Kashmir, India. [13]Leipzig Institute for Meteorology (LIM), Leipzig University, Leipzig, Germany. [14]Department of Environmental Science and Engineering, Indian Institute of Technology (ISM) Dhanbad, Dhanbad, India.

*Address correspondence to: basudev.swain@physics.ox.ac.uk

Citation: Swain B, Vountas M, Singh A, Panda U, Song R, Anchan NL, Malasani CR, Mallick D, Alawode R, Deroubaix A, et al. Contrasting Anthropogenic Drivers Behind Asymmetric Warming in the Arctic and Antarctica. *Ocean-Land-Atmos. Res.* 2026;5:Article 0127. https://doi.org/10.34133/olar.0127

Submitted 29 July 2025
Revised 27 October 2025
Accepted 27 November 2025
Published 8 January 2026

Surface air temperature (SAT) in polar regions is rising faster than the global average. This study analyzes the rapid increase in anthropogenic influences throughout the industrial period on Arctic and Antarctic warming, utilizing climate models. Our results show that while the SAT trend in the Arctic due to greenhouse gas (GHG) forcing is approximately 0.6 °C/decade, twice that of land use (LU) forcing at 0.3 °C/decade, the amplification of Arctic warming from LU forcings (with an amplification factor of 2.37) is stronger than the GHG forcings (amplification factor of 2.25). Anthropogenic aerosols cool the Arctic 1.5 times more than Antarctica, driven by higher aerosol concentrations from long-range pollutant transport from lower latitudes. Since 1950, rapid industrialization in the Northern Hemisphere has caused Arctic warming to accelerate, with SAT rising by 0.34 °C/decade due to anthropogenic forcings—over twice the global average of 0.17 °C/decade. In contrast, Antarctic warming has remained closer to global trends, buffered by its remoteness from the anthropogenic influence. Under the high-emission scenario (RCP8.5), both polar regions are projected to experience substantial temperature increases by the end of the 21st century, underscoring the significant role of human activities in polar warming and the need for targeted interventions addressing regional and global changes in LU, GHG emissions, and anthropogenic aerosols.

Introduction

In recent decades, the rapid rise in surface air temperature (SAT) in the Arctic and Antarctica has become a central topic of climate research [1–5]. These polar regions, highly sensitive to ongoing global warming, play a critical role in the Earth's climate system [3]. Accelerated melting of polar ice contributes significantly to the rise of sea level, with broad implications for ecological and environmental processes worldwide [1,6–9].

The pronounced rise in regional and global SAT results from a complex interplay of natural and anthropogenic forcings [1,3]. Since the pre-industrial period (1850–1900), global mean SAT has increased by approximately 1.09 °C [10], but polar warming reveals distinct spatial and temporal patterns. The Arctic, in

particular, is experiencing warming at rates up to 4 times compared to global average, a phenomenon that is acknowledged as Arctic amplification (AA) [1], although the magnitude of this amplification varies depending on the time period analyzed. In contrast, the rise of the Antarctic SAT is more heterogeneous, with stronger increases observed over the Antarctic Peninsula and some parts of western Antarctica compared to the eastern part [3]. Notably, the Arctic's accelerated warming outpaces that of mid-latitude northern regions as well as the Southern Hemisphere and tropics, emphasizing the urgent need to understand the drivers behind these regional disparities.

Despite extensive research [1,11–20], a comprehensive assessment quantifying the distinct industrial period anthropogenic contributions to warming in both polar regions remains limited. In particular, previous studies have not fully isolated how different human-induced forcings, greenhouse gases (GHGs), anthropogenic aerosols, and land-use (LU) changes, have variably influenced Arctic and Antarctic temperature trends.

This study addresses this gap by investigating how the rapid intensification of anthropogenic activities since the start of the industrial period (1955–2005) has differentially affected warming in the Arctic and Antarctic with respect to the pre-industrial baseline (1850–1900) [10]. We use the Coupled Model Intercomparison Project Phase 5 (CMIP5) ensemble [21], which offers a rich suite of climate model output datsets, including historical single-forcing experiments that isolate the effects of GHGs, aerosols, and critically the land-use changes (see Table S1). These simulations, widely used in Intergovernmental Panel on Climate Change (IPCC) assessments [22], span from the pre-industrial era to future scenarios, allowing rigorous attribution of polar warming to specific forcings.

Our analysis reveals several key insights; first, the Arctic has experienced a markedly faster warming rate than the global average during the industrial period, driven primarily by GHG forcing but also significantly influenced by land-use changes. Second, although GHGs produce the largest absolute warming in the Arctic (approximately 0.6 °C/decade), the amplification factor associated with LU forcing exceeds that of GHGs (2.37 versus 2.25), underscoring the important role of land use (LU) change in AA. Importantly, prior studies [1,11–20] on polar warming have generally overlooked land-use forcing, limiting a full understanding of anthropogenic impacts.

Materials and Methods

This study examines 158 output datasets of 22 CMIP5 models [21] for various anthropogenic as well as natural single forcings (see Table S1) for the historical period from 1850 to 2005. Climate models replicate past and present climate conditions by incorporating various components, including greenhouse gas emissions, volcanic eruptions, and human-related emissions. According to the IPCC's Fifth Assessment Report [23–25], these experiments are essential to the CMIP5 coordinated efforts. For our analysis, we used multiple ensembles with monthly mean SAT outputs across 4 scenarios Representative Concentration Pathway (RCP)2.6, RCP4.5, RCP6.0, and RCP8.5], alongside historical simulations (NAT, Aaer, GHGs, LU) with varying forcings (see Table S1). RCP4.5 corresponds to a radiative forcing of 4.5 W / m^2 beyond 2100, indicating potential CO_2 emissions surpassing 650 ppm (parts per million). Similarly, RCP8.5 corresponds to 8.5 W/m^2 post-2100, suggesting CO_2 equivalents exceeding 1,370 ppm [24]. The SAT observations were obtained from the HadCRUT5 monthly average anomaly, weighted by area, adjusted by subtracting the long-timespan mean (1850–1900) to derive the anomaly. While interpreting primary data, the median of these observations and model data was taken into account. The SAT outputs were regridded to $1° \times 1°$ resolution by using climate data operators (CDOs) to make trend estimation easier [26]. Using iteratively reweighted least squares (IRLSs) [27], robust regression was used for trend analysis in order. This approach minimizes the effects of extreme values [28,29]. *t* Tests at 95% confidence were used [30] to estimate the significance of SAT changes.

Rationale for using CMIP5 in this study

While several previous studies [1,11–20] on AA have focused on rising temperatures in the Arctic and their associated climatic consequences, the primary objective of this study is to trace the influence of anthropogenic activities during the industrial period on historical warming across both the Arctic and Antarctic regions. Achieving this objective requires isolating the contributions of individual anthropogenic forcings, including GHGs, anthropogenic aerosols, and, critically, land-use (LU) changes. The CMIP5 [21] model ensemble provides a comprehensive suite of historical single-forcing experiments, including simulations specifically designed to isolate the effects of LU changes (see Table S1), thereby enabling a consistent and full-scale attribution analysis of the influence of each anthropogenic driver on polar SAT trends.

Although CMIP6 [23] includes single-forcing experiments for GHGs and aerosols, it does not provide LU-only single-forcing experiments. CMIP6 includes some different experiments for land-use-related simulations (e.g., land-hist, land-hist-altLu1, and land-hist-altLu2), which are limited to land-only model configurations and only account for temperature changes over land surfaces. As such, they do not capture the combined land–ocean SAT response to land-use changes and are therefore not suitable for our study.

It is important to note that CMIP6 includes a single-forcing experiment, hist-noLu (see Table S2), in which land-use forcing is fixed at pre-industrial levels. Subtracting hist-noLu from the full historical simulation provides an estimate of the combined effects of GHG and LU, anthropogenic aerosols, and natural forcings on SAT, but this difference does not isolate the LU contribution alone (Fig. 1A to C). Moreover, subtracting the GHG, Aaer, noLU, and NAT single-forcing simulations from the historical SAT does not yield the SAT attributable solely to LU forcing. This is because the sum of SAT anomalies from the individual single-forcing experiments does not equal the total historical SAT simulated by CMIP6 [10, 23, 31, 32,].

This non-additivity arises from the nonlinear interactions among different forcing agents within the coupled climate system. For instance, aerosols can modulate the radiative effects of GHGs through cloud-radiation feedbacks, and land-use changes can alter local energy balance and moisture fluxes, thereby influencing the temperature response to both GHGs and aerosols [23,31,32]. As a result, the climate response to combined forcings is not a linear superposition of the responses to each forcing applied independently. Hence, estimating the LU-induced SAT change requires explicit hist-Lu simulations or dedicated factorial experiments that account for these nonlinear feedbacks. While CMIP6 extends historical simulations up to 2014 (compared to 2005 in CMIP5), the additional 9 years of data do not significantly enhance the long-term attribution of anthropogenic impacts, especially in the absence of comprehensive LU forcing experiments.

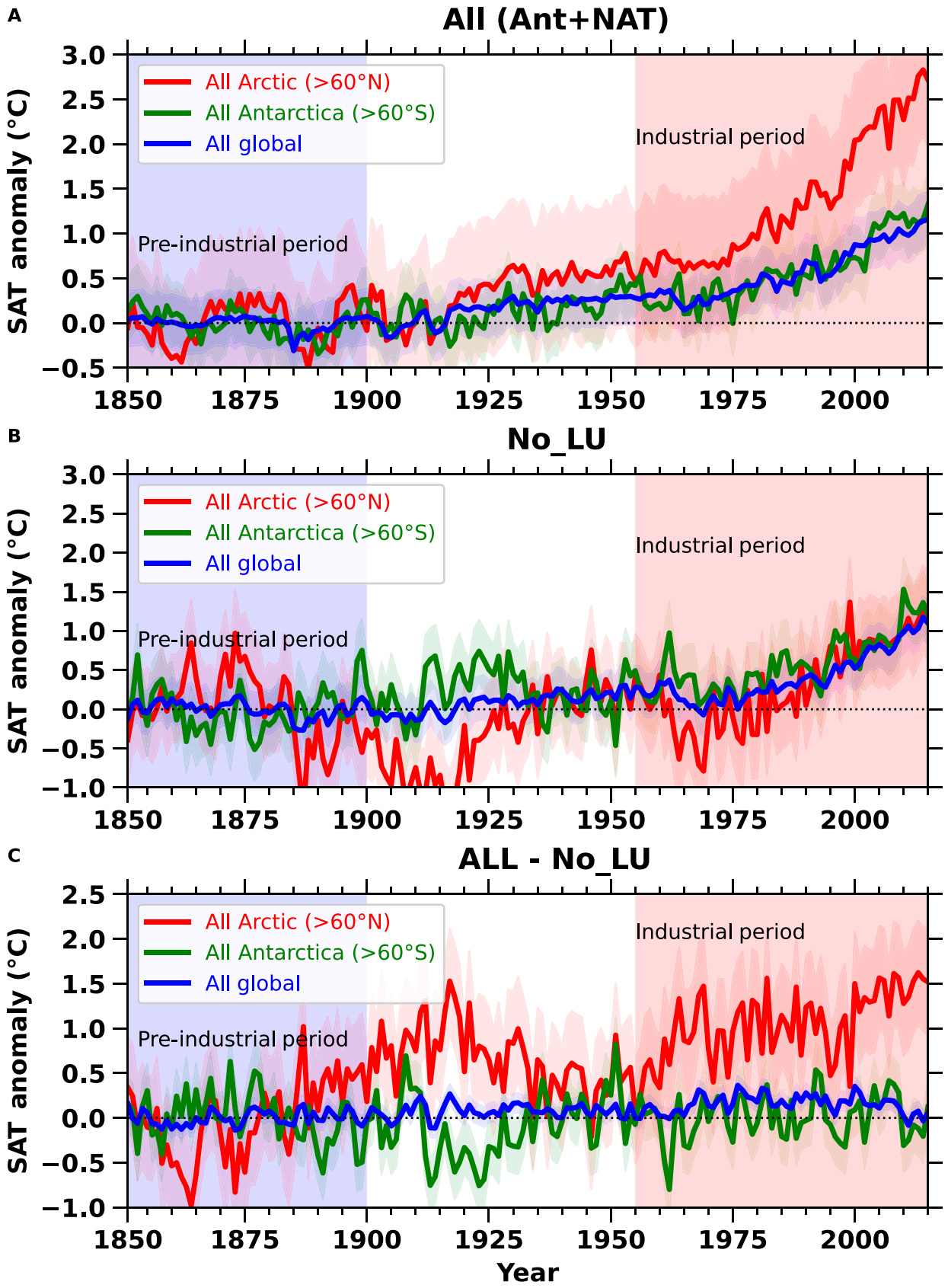

Fig. 1. Changes in SAT due to no-LU forcings over the Arctic, Antarctica, and globally. The annual anomaly of the SAT due to no-LU influences over the pre-industrial (1850–1900) to industrial period (1955–2014) from CMIP6 simulations is presented for Arctic (red), Antarctica (green), and globally (blue). The anomaly for different SATs is calculated with respect to the baseline from 1850 to 1900. Historical SAT anomalies for all forcings (A), without land-use forcing (B), and no land-use forcing subtracted from all forcings (C).

Therefore, for the purposes of conducting a scientifically robust and comprehensive assessment of human-induced polar warming, including the critical influence of land-use changes, CMIP5 remains the most suitable and consistent framework for the present study. Using CMIP5 restricts the inclusion of recent accelerated warming trends in the Arctic, but the results presented provide a robust attribution of anthropogenic influences over the industrial period where all forcings can be fully evaluated.

Calculation of polar amplification factors

To quantify the magnitude and spatial distribution of local amplification factors over the polar regions, as well as the AA, the amplification factor is calculated at each grid point within the Arctic and Antarctic domains. The amplification factor is characterized as the ratio of the local SAT trend at each grid point to the global mean SAT trend over the same time period.

The amplification factor A at each grid point (x,y) is calculated as:

$$A(x,y) = \frac{\Delta T_{\text{local}}(x,y)}{\Delta T_{\text{global}}} \quad (1)$$

where $\Delta T_{\text{local}}(x,y)$ is the SAT trend at each grid point due to individual forcings (x,y), and ΔT_{global} is the spatially averaged global SAT trend for the same period due to individual forcings.

Trends were calculated using the CDO trend function over 2 distinct periods, the pre-industrial period (1850–1900) and the industrial period (1955–2005). To ensure statistical significance of SAT trends, all grid points with nonsignificant trends ($P > 0.1$) were masked prior to the calculation of the amplification factor. This approach ensures a robust and spatially explicit representation of local polar amplification patterns. Similarly, amplification factors were also computed separately for each individual anthropogenic forcing (e.g., GHGs, aerosols, and land-use changes) using the same methodology, enabling attribution of their specific contributions to the local amplification for polar regions.

Results and Discussion

Rising anthropogenic impacts over time on polar warming

There is a high degree of consistency between the CMIP5 estimations for both polar regions over the past 50 years and the 2 observational datasets (HadCRUT5 [33] and ERA5 [34]) (Fig. 1A and B). Plotting the multi-model-mean (MMM) anomaly of SAT due to different forcings from 1850 to 2005 allows us to evaluate the contributions of each individual forcing to the polar warming, as shown in Fig. 2A to F, for the Arctic, Antarctica, and the global average SAT. As polar warming (PW) is considered with respect to global warming, the global average SAT anomaly for different forcings is also depicted in Fig. 2A to F as a reference. The annual mean SAT for the pre-industrial era (1850–1900) is subtracted from the annual mean for both poles and the world from January 1850 to December 2005 to determine the temporal anomalies. Each figure shows the regression fits and the ensemble boundaries (maximum and minimum values).

Figure 2A shows an increase in total SAT over the Arctic beginning around 1900, while SAT over Antarctica largely follows global warming. The year 1900 marks a critical transition

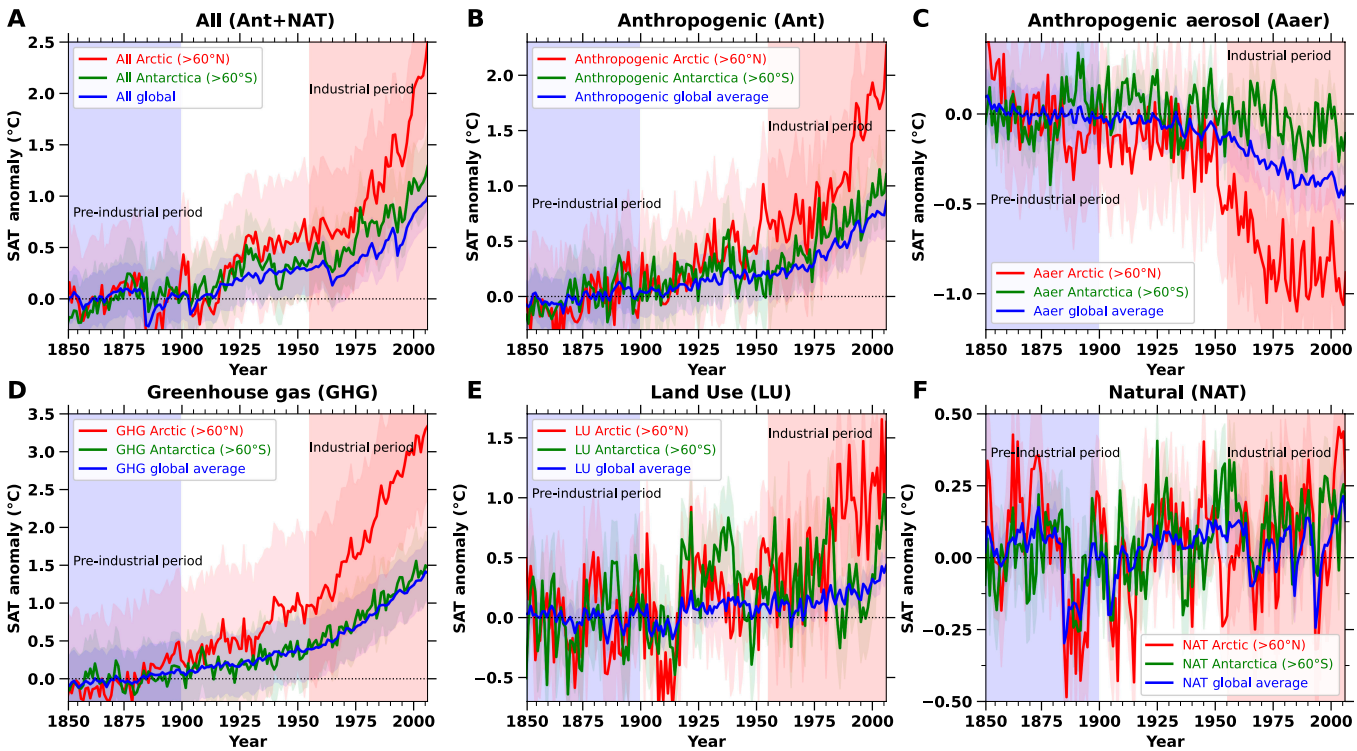

Fig. 2. Changes in SAT due to different forcings over the Arctic, Antarctica, and globally. The annual anomaly of the SAT due to different human-driven (anthropogenic) and natural influences over the pre-industrial (1850–1900) to industrial period (1955–2005) is presented for Arctic (red), Antarctica (green), and globally (blue). The anomaly for different SATs is calculated with respect to the baseline from 1850 to 1900. Historical SAT anomalies for all forcings (A), anthropogenic forcings (B), anthropogenic aerosol forcing (C), greenhouse gas forcing (D), land-use forcing (E), and natural forcings (F).

point in the mean annual SAT anomaly time series, shifting from negative to positive anomalies (Fig. 2A). Following this date, all forcings combined (Ant + NAT) (Fig. 2A) as well as individual forcings such as GHG and Ant (Fig. 2B and D) exhibit a notable rise in SAT. Land-use (LU) forcing contributes a more pronounced warming at the beginning of 1955 (Fig. 2E). Contrarily, Aaer exerts a strong cooling effect after 1950 (Fig. 2C), and natural forcings (NAT) display minimal impact on SAT anomalies (Fig. 2F).

Considering GHG and LU alone results in a high estimate of Arctic warming during the industrial period, while Antarctica follows the global warming trend for these forcings (Fig. 2D and E). The warming attributed to GHG shows a notable increase after 1950 in the Arctic, consistent with LU forcings (Fig. 2D and E). Additionally, anthropogenic effects become apparent post-1950, marking the start of the rapid increase in the industrial period anthropogenic activities (Fig. 2B). The CMIP5 model estimations indicate a slight overall rise in SAT attributed to anthropogenic factors before the 1950s (Fig. 2B), suggesting that nearly all anthropogenic warming over the Arctic has occurred since then (Fig. 2B).

The Aaer forcing demonstrates a significant cooling in SAT from 1925 onward over the Arctic and globally, with lesser impact on Antarctica (Fig. 2C). Over time, the impacts of NAT (solar radiation + volcanic eruptions) forcings on SAT are smaller compared to GHG and LU, but Antarctica experiences a higher NAT forcing than the Arctic and globally (Fig. 2F). This is mainly due to the greater impact of volcanic eruptions on Antarctica compared to the Arctic [35]. The findings indicate that anthropogenic aerosols significantly contributed to the cooling of the Arctic, with maximum anomaly reached up to −1 °C, thereby slowing the region's warming (Fig. 2C). Meanwhile, lesser reduction in SAT impact of Aaer in Antarctica is observed with anomaly reaching maximum of −0.1 °C (Fig. 2C). Further, the larger fluctuations in LU-forced simulations arise from the inherently spatially heterogeneous nature of land-use forcing, which operates locally through changes in surface albedo, evapotranspiration, and roughness rather than as a globally uniform radiative perturbation [31,36,37]. Because the LU-induced temperature signal is small relative to internal climate variability, especially in high-latitude regions, it is more easily masked by natural variability when averaged across limited ensemble members. Moreover, differences in land-surface parameterizations, vegetation distributions, and land-use datasets among CMIP6 models contribute to substantial intermodel spread. The smaller ensemble size available for LU experiments further limits the ability to filter out unforced variability, amplifying apparent fluctuations compared to other forcings such as GHGs or aerosols.

These results further show the strong outcome of direct anthropogenic contribution to the Arctic compared to Antarctica since the onset of industrialization, compared to the pre-industrial era, triggered the intense Arctic warming, while Antarctica follows the global warming.

Anthropogenic influence on local polar amplification factor

The spatial distribution of Arctic and Antarctica warming during the industrial period was investigated using the HadCRUT5, NOAA, and ERA5 observational datasets, shown in Figs. S1A and B and S2A and B, respectively. They show that a significant portion of the Arctic Ocean is heating faster at the rate of 0.4 °C/decade (Fig. S1A), whereas the peninsular region and Weddell Sea region of Antarctica is warming at the rate of 0.25 °C/decade (Fig. S2A). Thus, the ocean region of the Arctic and peninsular region, and the Weddell Sea region of Antarctica are warming faster than the global average, which can be seen in the local amplification factors presented in Figs. S1B and S2B, respectively. The amplification factor is estimated by dividing the temperature trends over poles as depicted in Fig. S1A by the ensemble global mean SAT trend at each grid point, and then we obtained the spatial map of the local PW amplification factor for Arctic and Antarctic, respectively (Figs. S1B and S2B).

The historical forcings were decomposed into constituent parts identified as trends during the pre-industrial (1850–1900) and industrial period (1955–2005) for Arctic (Fig. S3A and B) and Antarctica (Fig. S4A and B), as well as associated local AA factors of the Arctic (Fig. 3A and B) and Antarctica (Fig. S4C and D). By dividing the temperature trends depicted in Fig. S1A by the ensemble global mean SAT trend (Fig. S3A and B) at each point on the grid, we obtained the spatial map of the local PW amplification factor for Arctic and Antarctica [1] over the course of both pre-industrial and industrial eras for areas north of Arctic circle (Fig. 3A and B) and Antarctica regions (Fig. S4C and D). Values of more than one signify regions where warming is occurring more rapidly compared to the global average, whereas values of less than one indicate areas where the warming rate is lower [1].

The HadCRUT5, NOAA, and ERA5 SAT observations and the CMIP5 MMM consistently reveal that a major share of the Arctic Ocean experienced accelerated warming during the industrial period, with a trend of approximately 0.38 °C/decade (Fig. S1B), in stark contrast to the weaker and negative trend observed during the pre-industrial period, at −0.06 °C/decade (Fig. 4A). This corresponds to a local amplification factor of about 2.3 over the Arctic region (Fig. 4B).

In contrast, central Antarctica closely followed the global warming trend, with an average SAT increase of 0.11 °C/decade during the industrial period. This is evident when comparing spatial SAT trends between the periods before and during industrialization (Fig. S4A versus Fig. S4B).

Continental land areas such as North America, the Canadian archipelago, Western Siberia, the Eurasian sector, and areas surrounding Svalbard also exhibited statistically significant warming trends during the industrial period (Fig. S3A and B). These regions, mostly located in lower Arctic latitudes, play a crucial role in enhancing the AA signal, as reflected in the amplification factor patterns (Fig. 3B). It is also important to note that land-use changes had negligible impact during the pre-industrial period (Fig. 3A), while their influence became highly significant in the industrial era, contributing notably to polar SAT increases (Fig. 3B).

The Weddell Sea region of Antarctica displayed statistically significant warming trends during the industrial period that were absent in the pre-industrial baseline (Fig. S4A versus Fig. S4B). When comparing spatial SAT trends across different observational datasets, all 3 sources showed broadly similar warming patterns. However, HadCRUT5 and NOAA exhibited slightly lower warming magnitudes than ERA5 in both polar regions (Fig. S2A and B).

Analyzing the individual forcings is crucial for accurately attributing the human influence on the accelerated warming observed over the central Arctic Ocean and the Weddell Sea over the course of the industrial period, with respect to the

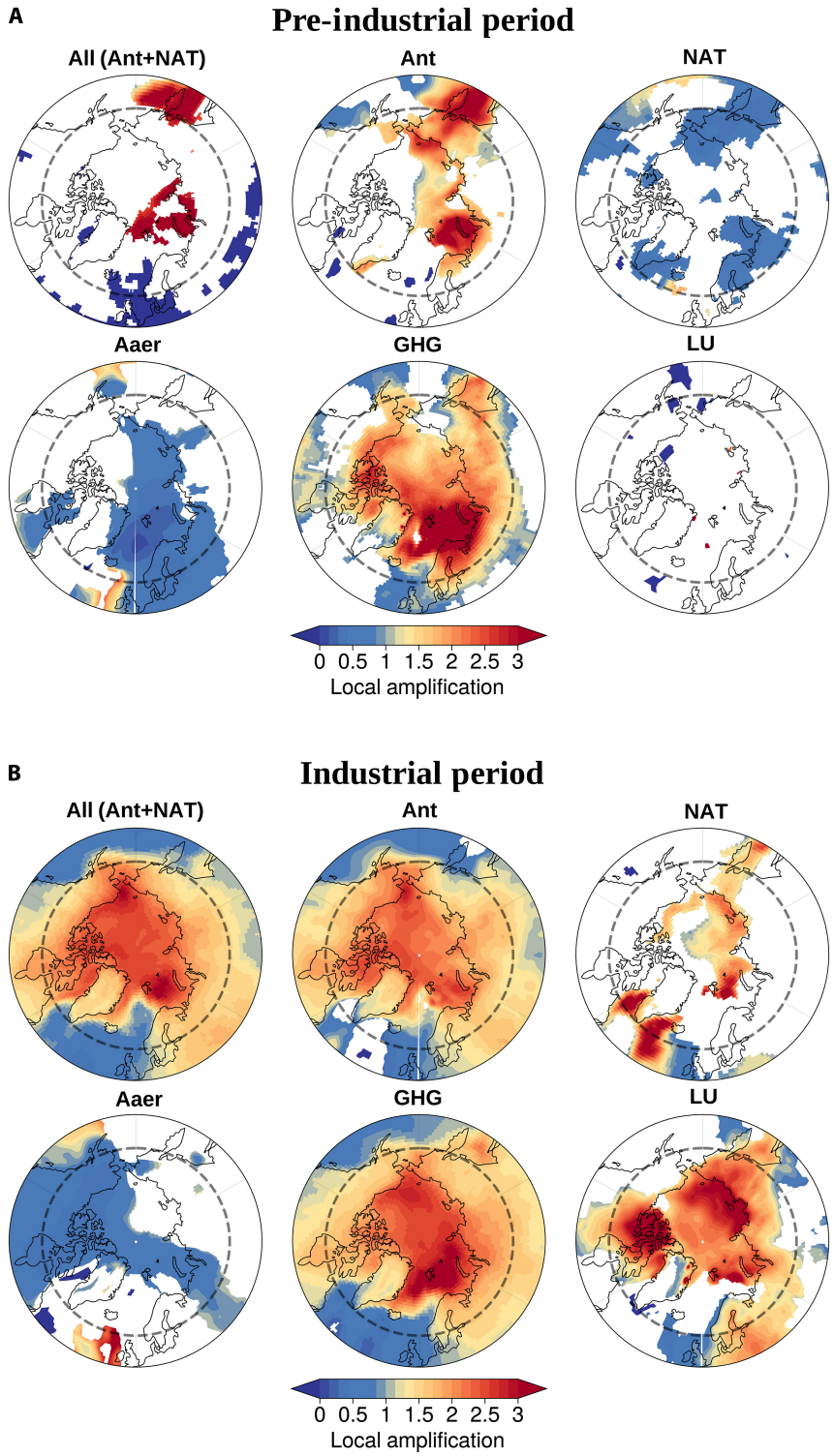

Fig. 3. Pre-industrial (1850–1900) and industrial (1955–2005) local AA factor for various forcings are presented geographically. The local polar amplification factor of multiple drivers associated with the Arctic is shown throughout the pre-industrial era (A) and industrial era (B). The trends that are not significant are omitted (white space) in these figures, and only significant trends are considered.

pre-industrial baseline (Fig. 4A and B). In the Arctic region, SAT grew sharply over the course of the industrial era due to various forcings. The combined anthropogenic and natural forcings (Ant + NAT) led to a rise in SAT trends from 0.11 °C/decade in the pre-industrial period to 0.33 °C/decade in the industrial period, associated with a local amplification factor of 2.02. Natural forcings (NAT) alone contributed a relatively minor change, with SAT trends ranging from −0.09 to 0.07 °C/decade, corresponding to an amplification factor of 1.73. The Aaer caused a reduction in temperature, with SAT trends between −0.14 and −0.11 °C/decade and a much lower amplification factor of 0.40. GHGs had a strong warming effect, with trends increasing

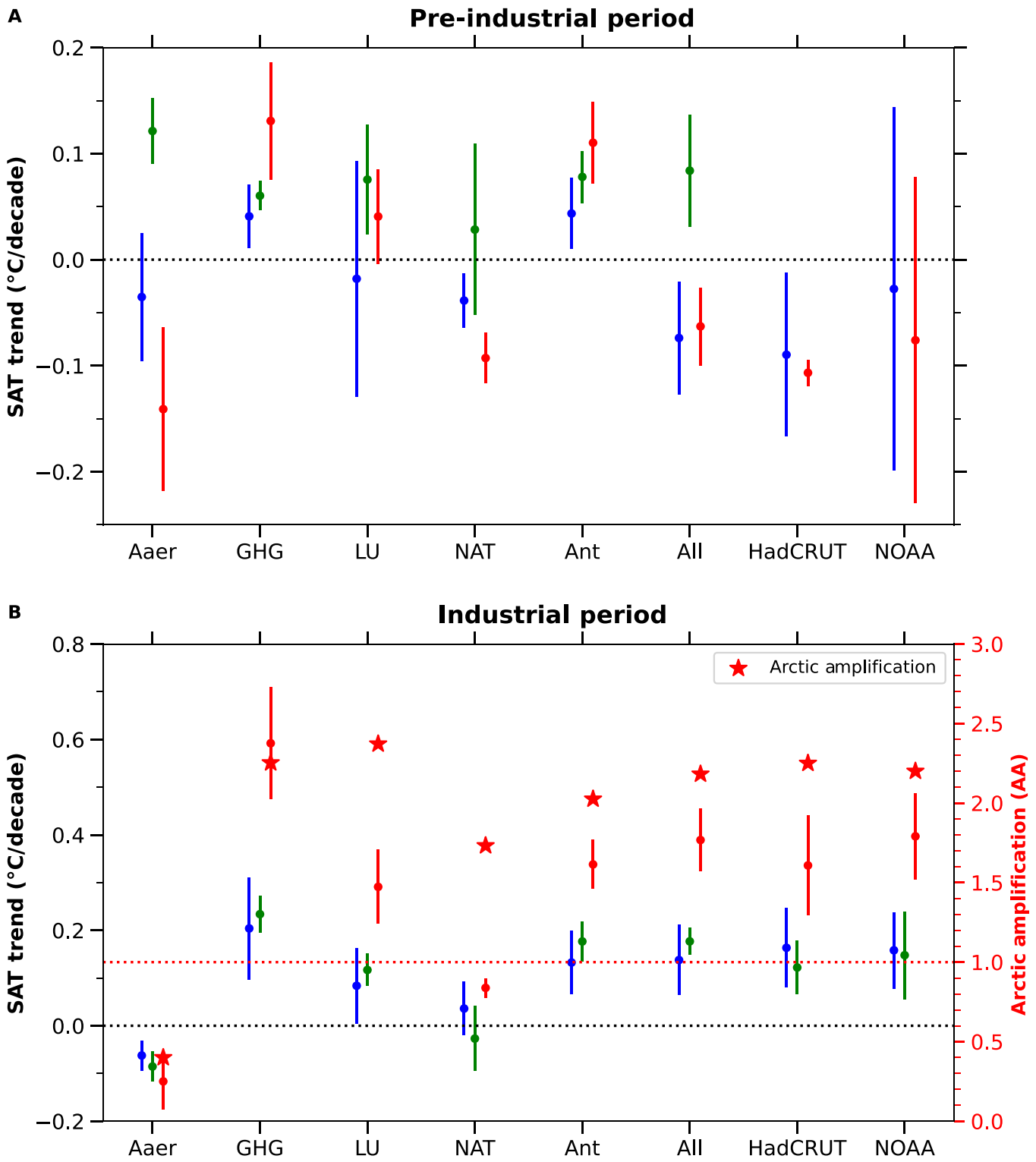

Fig. 4. Pre-industrial (1850–1900) and industrial period (1955–2005) significant SAT trends for Arctic, Antarctic, and global, and associated AA factors. The trend of different factors associated with the Arctic, Antarctica, and global is illustrated as (A) corresponding to the pre-industrial period and (B) corresponding to the industrial period, and associated AA factors. Red, green, and blue represent Arctic, Antarctica, and Global anomaly, respectively. The average of the significant trends is considered, and insignificant trends are removed.

from 0.13 to 0.60 °C/decade and an associated amplification factor of 2.25. Land-use changes (LU) also played a notable role, with SAT trends ranging from 0.04 to 0.30 °C/decade and a corresponding amplification factor of 2.37. Moreover, the Aaer's cooling role in the Arctic is 1.5 times stronger than in Antarctica (Fig. 4B), mainly due to the greater accumulation of these aerosols from the long-range transport of pollutants originating from lower latitudes [38]. Meanwhile, the cooling impact of anthropogenic aerosols in

Antarctica aligns with the global cooling trend of −0.08 °C/decade (Fig. 4B). These results underscore the varying contributions of each forcing and highlight the necessity of disentangling their individual effects to better understand the mechanisms driving polar amplification during the industrial era.

It is important to note that although the SAT trend over the Arctic due to GHG forcing (0.6 °C/decade) is 2 times than LU forcing (0.3 °C/decade), the AA factor due to LU forcings (i.e., amplification factor is 2.37) is stronger than the GHG forcing (i.e., amplification factor is 2.25). In contrast, Antarctica closely follows global warming trends, with SAT increases ranging from 0.07 to 0.17, 0.02 to −0.02, 0.12 to −0.08, 0.06 to 0.23, and 0.07 to 0.11 °C/decade due to Ant, NAT, Aaer, GHG, and LU forcings.

This highlights the greater influence of human actions on central Arctic warming, mainly by emitting GHG, followed by

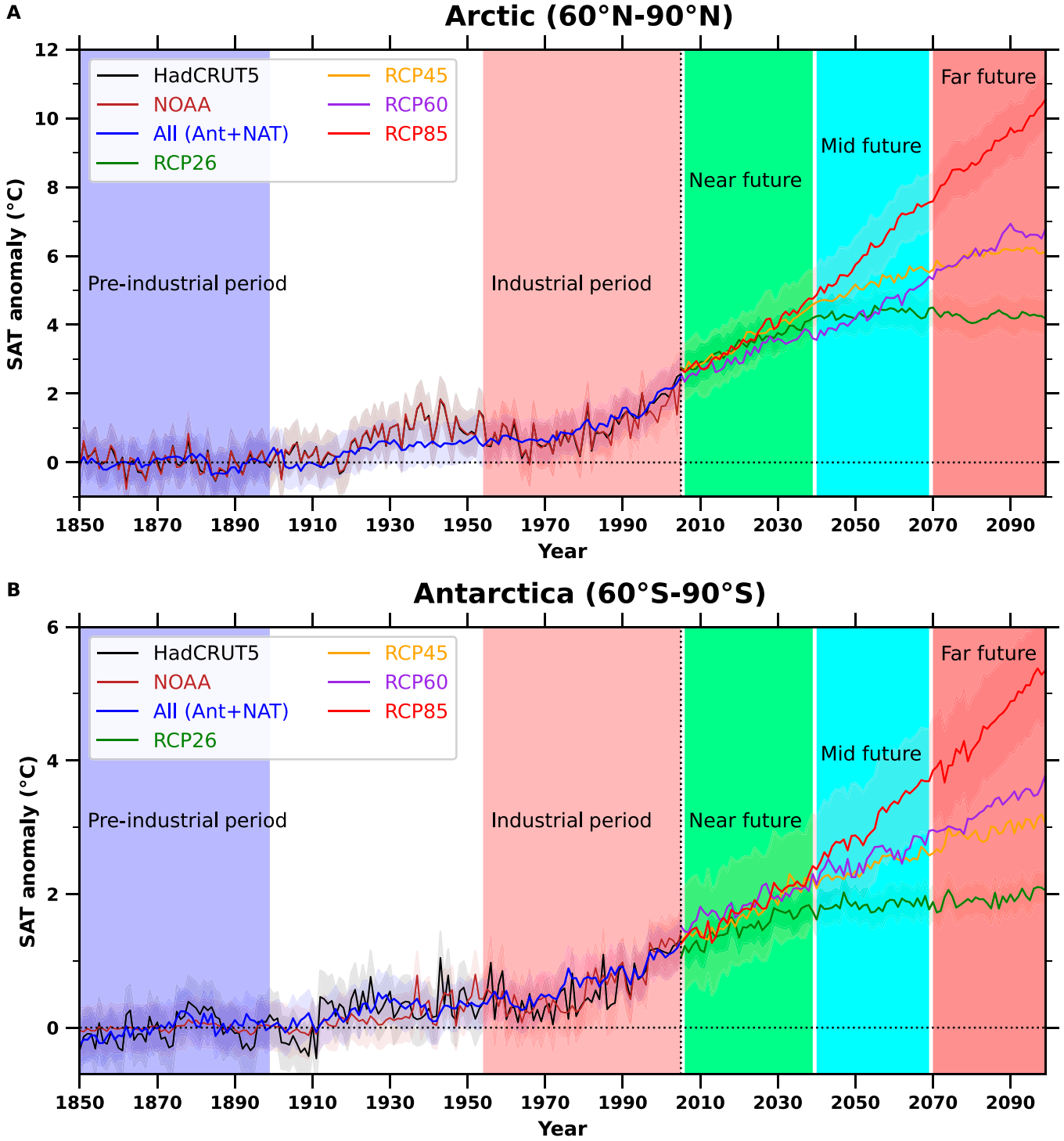

Fig. 5. The SAT anomalies from 1850 to 2100 are presented for Arctic and Antarctica. The MMM SAT anomaly together with the SAT observations (HadCRUT5 and NOAA) is presented from the past to the future (different RCP scenarios). The anomaly is calculated with respect to the baseline timespan (1850–1900). Historical SAT and future SAT anomalies for Arctic (A) and Antarctica (B).

regional and global LU effects (Fig. 3A and B). Notably, Aaer forcing triggered a decrease in SAT over Eurasian and northern Siberian regions over the pre-industrial era [Fig. 3A(iv)] and over the North American geographic area throughout the industrial era [Fig. 3B(iv)]. NAT forcing had a negligible impact during the pre-industrial [Fig. 3A(iii)] and industrial period [Fig. 3B(iii)]. The increase in SAT due to LU forcings over central Arctic Oceanic regions and continental areas of Eurasia and northern Siberia during the industrial period [Fig. 3B(vi)] can be attributed to the indirect impact of LU forcings at low

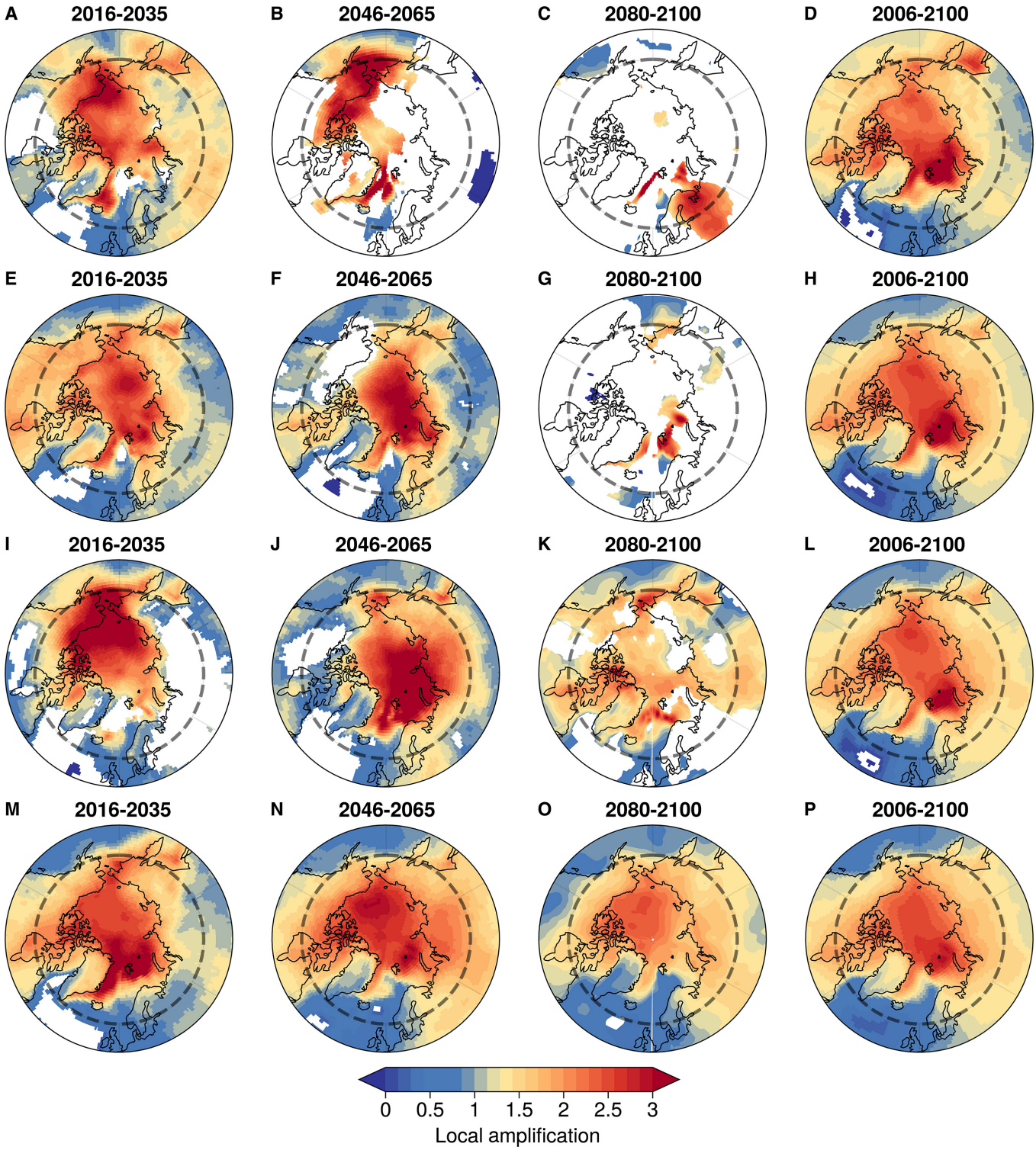

Fig. 6. Future rise in local amplification factors over the Arctic for 4 future scenarios (such as RCP2.6, RCP4.5, RCP6.0, and RCP8.5). Future local amplification factors for the Arctic spatially presented as (A) for RCP2.6, (B) for RCP4.5, (C) for RCP6.0, and (D) for RCP8.5 for near future (2006–2035), mid-future (2046–2065), and far future (2080–2100), as well as for the entire model simulation period (2006–2100). The local amplification factor is calculated by dividing the global average significant SAT trend with each grid cell of the Arctic region (≥60°N). Panels (E) to (P) shows future local polar amplification factors for different future timespans for different emission scenarios.

latitudes, influenced by atmospheric circulation patterns (Fig. 3A and B), consistent with the observations (Fig. S2A and B). During the industrial period, the boundary south of the Arctic circle (60°N to 75°N) showed local AA factors exceeding 3 due to all forcings [Fig. 3B(i)]. The amplification factor's magnitude increased toward the north of the Arctic circle, indicating a larger proportion of oceanic areas within this boundary where the local AA factor is most pronounced due to GHG [Fig. 3B(v)] and LU [Fig. 3B(vi)] forcings during the industrial period. Conversely, the Weddell Sea region of Antarctica experienced comparatively

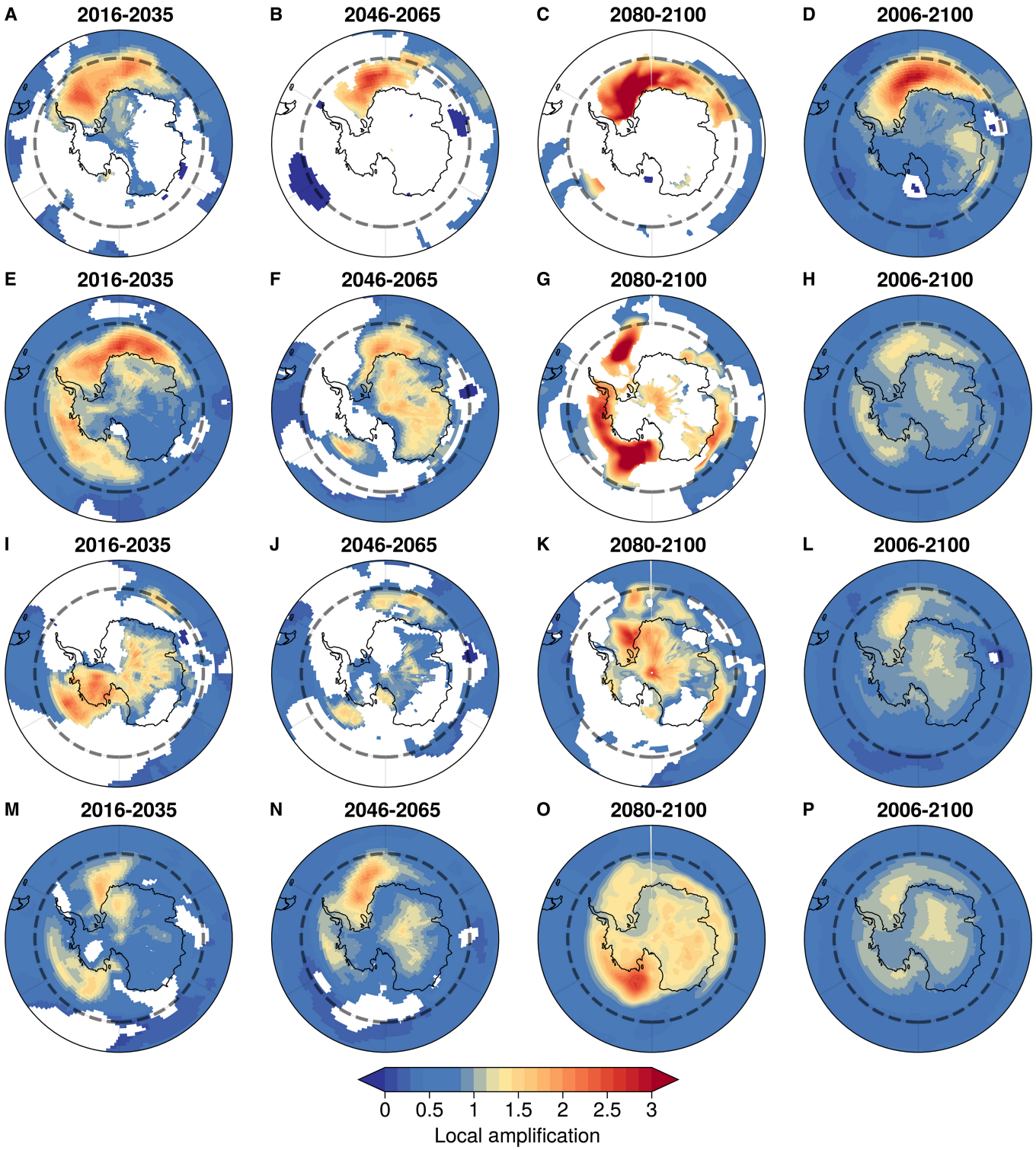

Fig. 7. Future rise in local amplification factors over Antarctica for 4 future scenarios (such as RCP2.6, RCP4.5, RCP6.0, and RCP8.5). Future local amplification factors for the Arctic spatially presented as (A) for RCP2.6, (B) for RCP4.5, (C) for RCP6.0, and (D) for RCP8.5 for near future (2006–2035), mid-future (2046–2065), and far future (2080–2100), as well as for the entire model simulation period (2006–2100). The local amplification factor is calculated by dividing the global average significant SAT trend with each grid cell of the Antarctica region (≥60°S). Panels (E) to (P) show future local polar amplification factors for different future timespans for different emission scenarios.

more warming than other parts of the region, primarily due to GHG and NAT forcings (Fig. S4D).

Future projections of polar warming

The observed rise in SAT at both poles, resulting from the combined effect of all forcings throughout the entire time period, aligned with recorded observational SAT datasets (Fig. 5A and B).

However, HadCRUT5 and NOAA data showed that an average warming of approximately 0.3 °C from the mid-20th century (1925–1950) contrasted with past CMIP5 models over the Arctic (Fig. 5A). A greater cooling effect of aerosol response in different climate models could be the cause of this disparity [39]. We feel comfortable forecasting Arctic and Antarctic warming in terms of an increase in SAT anomaly during the 21st century because the measurements and the multi-model mean are similar. We considered both low and high RCP emission scenarios (i.e., RCP2.6 to RCP8.5). By the end of the century, RCP2.6 and RCP8.5 show a temperature difference of approximately 7.2 °C over the Arctic and 3 °C over Antarctica (Fig. 5A and B).

In the Arctic, temperature projections under RCP8.5 show a consistent upward trend, while the projected mean temperature under RCP2.6 rises until around 2050, and then slightly declines, reflecting the radiative forcing pattern under RCP2.6. In Antarctica, RCP8.5 also indicates a continuous increase in temperatures, whereas RCP2.6 shows an increase until approximately 2050, followed by stabilization (Fig. 5A and B).

The spatial patterns of SAT trends (Figs. S5A to D and S6A to D) and the corresponding polar warming factors over the Arctic (Fig. 6A to P) and Antarctica (Fig. 7A to P) are projected throughout the 21st century, ranging from low-emission (RCP2.6) to high-emission (RCP8.5) scenarios. These trends were evaluated for separate intervals: the near-future (2006–2035), mid-future (2046–2065), and far-future (2080–2100), as well as for the entire model simulation period (2006–2100). In the Arctic, under RCP2.6, temperatures are expected to rise in the near future, but decrease in the mid- and far-future periods, resulting in an overall SAT increase of approximately 0.6 °C/decade, associated with an Arctic warming factor exceeding 2.3 (Fig. 6A to D). However, far-future projections suggest cooling across most of the Arctic, except for parts of Eurasia (Fig. 6A to D). In contrast, under the RCP8.5 scenario, SAT is projected to increase continuously in the near, mid-, and far-future, with the mid-21st century experiencing significantly higher temperatures than both the near and far future. Long-term trends (2006–2100) show a warming rate of about 1.2 °C/decade, with an associated Arctic warming factor greater than 3.1.

Over Antarctica, under RCP2.6, temperatures are projected to increase over the Weddell Sea region in the near future and decrease in both the mid- and far-future periods, with an overall increase in SAT of approximately 0.12 °C/decade (Fig. S6A to D), associated with an Antarctic warming factor of more than 1.2. Far-future projections indicate warming over most of the Antarctica region (Fig. 7A to P). Under the RCP8.5 scenario, continuous increases in SAT are anticipated in the mid- and far-future (Fig. 7D), with significantly higher temperatures projected for the late 21st century compared to the near and mid-future periods. Long-term trends (2006–2100) indicate a warming rate of approximately 0.5 °C/decade, accompanied by an Antarctic warming factor exceeding 1.3 (Fig. 7D).

Physical mechanisms of Arctic and Antarctica warming

The pronounced AA compared to the more moderate Antarctic warming arises from a combination of distinct regional factors and feedback processes. In the Arctic, the loss of sea ice and snow cover initiates strong positive feedbacks, most notably the ice–albedo feedback, whereby reduced surface reflectivity leads to enhanced solar absorption and further warming [2,40,41]. This is compounded by Arctic-specific atmospheric circulation patterns, changes in cloud cover, and ocean heat transport, all of which amplify local temperature increases beyond global averages [42,43].

In contrast, the Antarctic climate system is influenced by several factors that moderate warming trends. The Southern Ocean's circumpolar current acts as a thermal barrier, limiting the poleward transport of warm waters. Additionally, the extensive Antarctic ice sheet and persistent sea ice around much of the continent maintain a high-albedo surface, which dampens warming. Variability in stratospheric ozone and its recovery has also played a significant role in modulating atmospheric circulation patterns and surface temperatures over Antarctica [44]. Furthermore, regional differences within Antarctica, such as the more rapid warming observed on the Antarctic Peninsula and West Antarctica versus relative stability or cooling in East Antarctica, highlight complex interactions between oceanic, atmospheric, and cryospheric processes [45].

Conclusion

The analysis of various anthropogenic forcings not only provides insight into the overall contributions of each individual forcing to the observed polar warming but also shed light on their impact on SAT changes. Understanding how human activity affects the SAT of both poles in the face of growing industrialization and changing land cover dynamics requires knowledge of this information. Although GHG changes are expected to be the primary driver of future climate change, recent research has tended to ignore LU forcings in favor of GHG forcings. Previous estimations of LU, GHG, NAT, and aerosol-attributable warming and cooling in polar regions, particularly the significance of LU forcings relative to the pre-industrial period, have not been well investigated until now. Our findings show that while the SAT trend in the Arctic due to GHG forcing is 0.6 °C/decade—twice that of LU forcing at 0.3 °C/decade—the warming effect of LU forcings is stronger, with an amplification factor of 2.37, compared to 2.25 for GHG forcing. Furthermore, the Arctic experiences a notably stronger cooling effect from anthropogenic aerosols, approximately 1.5 times greater than that in Antarctica (Fig. 4B). This enhanced sensitivity is primarily due to the elevated levels of aerosol deposition in the Arctic, driven by long-range atmospheric transport of emissions from mid-latitude industrial regions [38].

The sharp rise in anthropogenic activities in the Northern Hemisphere since 1950 (the industrial era) has caused Arctic warming to accelerate at more than twice the rate of the global average. During this industrial period, the SAT in the Arctic increased by 0.34 °C/decade due to anthropogenic influences, compared to a global SAT rise of 0.17 °C/decade driven by the same factors (Fig. 4B). In contrast, Antarctic warming has remained more in line with global trends, as its distance from major sources of anthropogenic influence, such as LU changes, and its surrounding Southern Ocean buffer it from these effects.

Our study provides valuable insights into rapid rise of industrial period anthropogenic forcings on Arctic and Antarctic warming. Taken together, our findings demonstrate the substantial influence of anthropogenic-induced changes in LU, GHG, and anthropogenic aerosols, emphasizing the need to address these factors to mitigate polar warming during the rapidly increasing human activities during the ongoing industrial period.

Acknowledgments

We express gratitude to the CMIP5 model community for sharing their data. We further thank F. Pithan of Alfred Wegener Institute, Helmholtz Centre for Polar and Marine Research (AWI), Bremerhaven/Potsdam, Germany, for his valuable suggestions, which was very much helpful to shape the manuscript.
Funding: This research has received funding from the University and the state of Bremen, as well as from the Deutsche Forschungsgemeinschaft (DFG, German Research Foundation) under the project "ArctiC Amplification: Climate Relevant Atmospheric and Surface Processes, and Feedback Mechanisms (AC)3" as part of the Transregional Collaborative Research Center (TRR) 172, Project-ID 268020496.
Author contributions: B.S. and M.V. conceived and designed the research undertaken in this study. B.S. analyzed the datasets and generated the plots. B.S. led the analysis of results and wrote the manuscript with the help of M.V. All the co-authors helped in shaping the manuscript. All authors contributed to the interpretation of the results and the preparation of the final manuscript.
Competing interests: The authors declare that they have no competing interests.

Data Availability

All the CMIP5 model datasets are available at https://esgf-data.dkrz.de/search/cmip5-dkrz/. Observational data from HadCRUT5 are available at https://crudata.uea.ac.uk/cru/data/temperature/. ERA5 data are available at https://cds.climate.copernicus.eu/cdsapp#!/dataset/reanalysis-era5-single-levels?tab=overview. Observational data from NOAA are available at https://zenodo.org/records/3634713.

Supplementary Materials

Tables S1 and S2
Figs. S1 to S6

References

1. Rantanen M, Karpechko AY, Lipponen A, Nordling K, Hyvärinen O, Ruosteenoja K, Vihma T, Laaksonen A. The Arctic has warmed nearly four times faster than the globe since 1979. *Commun Earth Environ*. 2022;3(1):168.
2. Huang J, Zhang X, Zhang Q, Lin Y, Hao M, Luo Y, Zhao Z, Yao Y, Chen X, Wang L, et al. Recently amplified Arctic warming has contributed to a continual global warming trend. *Nat Clim Chang*. 2017;7(12):875–879.
3. Xie A, Zhu J, Kang S, Qin X, Xu B, Wang Y. Polar amplification comparison among earth's three poles under different socioeconomic scenarios from cmip6 surface air temperature. *Sci Rep*. 2022;12(1):Article 16548.
4. Post E, Alley RB, Christensen TR, Macias-Fauria M, Forbes BC, Gooseff MN, Iler A, Kerby JT, Laidre KL, Mann ME, et al. The polar regions in a 2 C warmer world. *Sci Adv*. 2019;5(12):eaaw9883.
5. Fasullo JT, Tilmes S, Richter JH, Kravitz B, MacMartin DG, Mills MJ, Simpson IR. Persistent polar ocean warming in a strategically geoengineered climate. *Nat Geosci*. 2018;11(12):910–914.
6. Wunderling N, Willeit M, Donges JF, Winkelmann R. Global warming due to loss of large ice masses and Arctic summer sea ice. *Nat Commun*. 2020;11(1):5177.
7. Smetacek V, Nicol S. Polar ocean ecosystems in a changing world. *Nature*. 2005;437(7057):362–368.
8. Bintanja R, Andry O. Towards a rain-dominated Arctic. *Nat Clim Chang*. 2017;7(4):263–267.
9. McCrystall MR, Stroeve J, Serreze M, Forbes BC, Screen JA. New climate models reveal faster and larger increases in Arctic precipitation than previously projected. *Nat Commun*. 2021;12(1):6765.
10. Gillett NP, Kirchmeier-Young M, Ribes A, Shiogama H, Hegerl GC, Knutti R, Gastineau G, John JG, Li L, Nazarenko L, et al. Constraining human contributions to observed warming since the pre-industrial period. *Nat Clim Chang*. 2021;11(3):207–212.
11. Zhou W, Leung LR, Xie S-P, Lu J. An analytic theory for the degree of Arctic amplification. *Nat Commun*. 2024;15(1):5060.
12. Zhou W, Leung LR, Lu J. Steady threefold Arctic amplification of externally forced warming masked by natural variability. *Nat Geosci*. 2024;17(6):508–515.
13. Ono J, Watanabe M, Komuro Y, Tatebe H, Abe M. Enhanced Arctic warming amplification revealed in a low-emission scenario. *Commun Earth Environ*. 2022;3(1):27.
14. Liang Y-C, Polvani LM, Mitevski I. Arctic amplification, and its seasonal migration, over a wide range of abrupt CO_2 forcing. *npj Clim Atmos Sci*. 2022;5(1):14.
15. Topál D, Ding Q. Atmospheric circulation-constrained model sensitivity recalibrates Arctic climate projections. *Nat Clim Chang*. 2023;13(7):710–718.
16. Fang M, Li X, Chen H, Chen D. Arctic amplification modulated by Atlantic multidecadal oscillation and greenhouse forcing on multidecadal to century scales. *Nat Commun*. 2022;13(1):1865.
17. Kim Y-H, Min S-K, Gillett NP, Notz D, Malinina E. Observationally-constrained projections of an ice-free Arctic even under a low emission scenario. *Nat Commun*. 2023;14(1):3139.
18. England MR, Polvani LM, Sun L, Deser C. Tropical climate responses to projected Arctic and Antarctic sea-ice loss. *Nat Geosci*. 2020;13(4):275–281.
19. Liu Z, Risi C, Codron F, He X, Poulsen CJ, Wei Z, Chen D, Li S, Bowen GJ. Acceleration of western Arctic sea ice loss linked to the Pacific North American pattern. *Nat Commun*. 2021;12(1):1519.
20. Naughten KA, Holland PR, De Rydt J. Unavoidable future increase in West Antarctic ice-shelf melting over the twenty-first century. *Nat Clim Chang*. 2023;13(11):1222–1228.
21. Taylor KE, Stouffer RJ, Meehl GA. An overview of CMIP5 and the experiment design. *Bull Am Meteorol Soc*. 2012;93(4):485–498.
22. Masson-Delmotte V, Zhai P, Pirani A, Connors SL, Péan C, Berger S, Caud N, Chen Y, Goldfarb L, Gomis MI, et al. IPCC, 2021: Summary for policymakers. In: *Climate Change 2021: The Physical Science Basis. Contribution of Working Group I to the Sixth Assessment Report of the Intergovernmental Panel on Climate Change*. Cambridge (UK): Cambridge University Press; 2021.

23. Eyring V, Bony S, Meehl GA, Senior CA, Stevens B, Stouffer RJ, Taylor KE. Overview of the coupled model intercomparison project phase 6 (CMIP6) experimental design and organization. *Geosci Model Dev*. 2016;9(5):1937–1958.
24. Van Vuuren DP, Edmonds J, Kainuma M, Riahi K, Thomson A, Hibbard K, Hurtt GC, Kram T, Krey V, Lamarque JF, et al. The representative concentration pathways: An overview. *Clim Chang*. 2011;109(1):5–31.
25. Pachauri RK et al. *Climate change 2014: Synthesis report. Contribution of Working Groups I, II and III to the Fifth Assessment Report of the Intergovernmental Panel on Climate Change*. Geneva (Switzerland): Intergovernmental Panel on Climate Change; 2014.
26. Schulzweid U, Kornblueh L, Quast R. *CDO user guide*. Hamburg (Germany): Max Planck Institute for Meteorology; 2019.
27. Holland PW, Welsch RE. Robust regression using iteratively reweighted least-squares. *Commun Stat Theor Meth*. 1977;6(9):813–827.
28. Yang H. The case for being automatic: Introducing the automatic linear modeling (LINEAR) procedure in SPSS statistics. *Gen Linear Model J*. 2013;39(2):27–37.
29. Kishore P, Basha G, Venkat Ratnam M, Velicogna I, Ouarda TB, Narayana Rao D. Evaluating cmip5 models using GPS radio occultation cosmic temperature in UTLS region during 2006–2013: Twenty-first century projection and trends. *Clim Dyn*. 2016;47(9):3253–3270.
30. Mishra P, Singh U, Pandey CM, Mishra P, Pandey G. Application of student's t-test, analysis of variance, and covariance. *Ann. Card. Anaesth*. 2019;22(4):407–411.
31. Lawrence DM, Hurtt GC, Arneth A, Brovkin V, Calvin KV, Jones AD, Jones CD, Lawrence PJ, de Noblet-Ducoudré N, Pongratz J, et al. The land use model intercomparison project (LUMIP) contribution to cmip6: Rationale and experimental design. *Geosci Model Dev*. 2016;9(9):2973–2998.
32. Shiogama H, Stone DA, Nagashima T, Nozawa T, Emori S. On the linear additivity of climate forcing-response relationships at global and continental scales. *Int J Climatol*. 2013;33(11).
33. Morice CP, Kennedy JJ, Rayner NA, Winn JP, Hogan E, Killick RE, Dunn RJH, Osborn TJ, Jones PD, Simpson IR. An updated assessment of near-surface temperature change from 1850: The hadcrut5 data set. *J Geophys Res Atmos*. 2021;126(3):Article e2019JD032361.
34. Hersbach H, Bell B, Berrisford P, Hirahara S, Horányi A, Muñoz-Sabater J, Nicolas J, Peubey C, Radu R, Schepers D, et al. The era5 global reanalysis. *Q J R Meteorol Soc*. 2020;146(730):1999–2049.
35. Verona LS, Wainer I, Stevenson S. Volcanically triggered ocean warming near the Antarctic peninsula. *Sci Rep*. 2019;9(1):9462.
36. Pitman AJ, de Noblet-Ducoudré N, Cruz FT, Davin EL, Bonan GB, Brovkin V, Claussen M, Delire C, Ganzeveld L, Gayler V, et al. Uncertainties in climate responses to past land cover change: First results from the lucid intercomparison study. *Geophys Res Lett*. 2009;36(14):Article 2009GL039076.
37. Rigden AJ, Li D. Attribution of surface temperature anomalies induced by land use and land cover changes. *Geophys Res Lett*. 2017;44(13):6814–6822.
38. Willis MD, Leaitch WR, Abbatt JP. Processes controlling the composition and abundance of Arctic aerosol. *Rev Geophys*. 2018;56(4):621–671.
39. Change I. Climate change 2007: The physical science basis. *Agenda*. 2007;6(07):333.
40. Wendisch M, Kirbus B, Ori D, Shupe MD, Crewell S, Sodemann H, Schemann V. Observed and modeled Arctic airmass transformations during warm air intrusions and cold air outbreaks. *Atmos Chem Phys*. 2025;25(21):15047–15076.
41. Wendisch M, Stapf J, Becker S, Ehrlich A, Jäkel E, Klingebiel M, Lüpkes C, Schäfer M, Shupe MD. Effects of variable, ice-ocean surface properties and air mass transformation on the Arctic radiative energy budget. *Atmos Chem Phys Discuss*. 2022;2022:1–31.
42. Screen JA, Simmonds I. Amplified mid-latitude planetary waves favour particular regional weather extremes. *Nat Clim Chang*. 2014;4(8):704–709.
43. Serreze MC, Barry RG. Processes and impacts of Arctic amplification: A research synthesis. *Glob Planet Chang*. 2011;77(1-2):85–96.
44. Turner J, Bracegirdle TJ, Phillips T, Marshall GJ, Hosking JS. An initial assessment of Antarctic sea ice extent in the cmip5 models. *J Clim*. 2013;26(5):1473–1484.
45. Stammerjohn SE, Martinson D, Smith R, Yuan X, Rind D. Trends in Antarctic annual sea ice retreat and advance and their relation to El Niño–Southern Oscillation and southern annular mode variability. *J Geophys Res Oceans*. 2008;113(C3):Article 2007JC004269.

Ocean - Land - Atmosphere Research
A SCIENCE PARTNER JOURNAL

Contrasting Anthropogenic Drivers Behind Asymmetric Warming in the Arctic and Antarctica

Basudev Swain, Marco Vountas, Aishwarya Singh, Upasana Panda, Rui Song, Nidhi L. Anchan, Chakradhar Reddy Malasani, Dukhishyam Mallick, Richard Alawode, Adrien Deroubaix, Luca Lelli, Julia Schmale, Ankit Tandon, Sachin S. Gunthe, Manfred Wendisch, Vittal Hari, and Hartmut Bösch

Citation: Swain B, Vountas M, Singh A, Panda U, Song R, Anchan N, Malasani C, Mallick D, Alawode R, Deroubaix A, et al. Contrasting Anthropogenic Drivers Behind Asymmetric Warming in the Arctic and Antarctica. *Ocean-Land-Atmos Res*. 2026;**5**:0127. DOI: 10.34133/olar.0127

Surface air temperature (SAT) in polar regions is rising faster than the global average. This study analyzes the rapid increase in anthropogenic influences throughout the industrial period on Arctic and Antarctic warming, utilizing climate models. Our results show that while the SAT trend in the Arctic due to greenhouse gas (GHG) forcing is approximately 0.6 °C/decade, twice that of land use (LU) forcing at 0.3 °C/decade, the amplification of Arctic warming from LU forcings (with an amplification factor of 2.37) is stronger than the GHG forcings (amplification factor of 2.25). Anthropogenic aerosols cool the Arctic 1.5 times more than Antarctica, driven by higher aerosol concentrations from long-range pollutant transport from lower latitudes. Since 1950, rapid industrialization in the Northern Hemisphere has caused Arctic warming to accelerate, with SAT rising by 0.34 °C/decade due to anthropogenic forcings—over twice the global average of 0.17 °C/decade. In contrast, Antarctic warming has remained closer to global trends, buffered by its remoteness from the anthropogenic influence. Under the high-emission scenario (RCP8.5), both polar regions are projected to experience substantial temperature increases by the end of the 21st century, underscoring the significant role of human activities in polar warming and the need for targeted interventions addressing regional and global changes in LU, GHG emissions, and anthropogenic aerosols.
Image

Ocean-Land-Atmosphere Research (ISSN 2771-0378) is published by the American Association for the Advancement of Science. 1200 New York Avenue NW, Washington, DC 20005.